Front. Optoelectron. 2019, 12(1): 88–96
https://doi.org/10.1007/s12200-017-0730-8

REVIEW ARTICLE

Detection of photonic orbital angular momentum with micro- and nano-optical structures

Chenhao WAN[1,2], Guanghao RUI[3], Jian CHEN[2,4], Qiwen ZHAN (✉)[2,5]

1 School of Optical and Electronic Information, Huazhong University of Science and Technology, Wuhan 430074, China
2 Department of Electro-Optics and Photonics, University of Dayton, 300 College Park, Dayton, Ohio 45469, USA
3 Advanced Photonics Center, Southeast University, Nanjing 210096, Jiangsu, China
4 School of Electronic Engineering, University of Electronic Science and Technology of China, Chengdu 611731, China
5 School of Optical-Electrical and Computer Engineering, University of Shanghai for Science and Technology, Shanghai 200093, China

Abstract Light with an optical orbital angular momentum (OAM) has attracted an increasing amount of interest and has found its way into many disciplines ranging from optical trapping, edge-enhanced microscopy, high-speed optical communication, and secure quantum teleportation to spin-orbital coupling. In a variety of OAM-involved applications, it is crucial to discern different OAM states with high fidelity. In the current paper, we review the latest research progress on OAM detection with micro- and nano-optical structures that are based on plasmonics, photonic integrated circuits (PICs), and liquid crystal devices. These innovative OAM sorters are promising to ultimately achieve the miniaturization and integration of high-fidelity OAM detectors and inspire numerous applications that harness the intriguing properties of the twisted light.

Keywords orbital angular momentum (OAM), optical vortices, singular optics, spatial light modulator, surface plasmon polariton (SPP), holography, photonic integrated circuit (PIC)

1 Introduction

It is well known that circularly polarized light carries spin angular momentum (SAM) [1]. Allen et al. recognized that, contrary to SAM which can only take one of the two values $\pm\hbar$, light with an azimuthal phase dependence of $\exp(il\varphi)$ carries an orbital angular momentum (OAM) that is characterized by $l\hbar$, where l is the topological charge (TC) that can be any integer [2]. Light with OAM has been intensively explored and applied to various applications including high-speed optical communications [3,4], optical spanners [5], edge-enhanced microscopy [6], and quantum optics [7,8]. To take full advantage of the intriguing property of dynamic rotation and the unbounded state space of OAM beams, it is crucial to develop highly efficient, compact, and high-resolution OAM sorters with parallel detection capabilities. Several methods based on conventional optical elements have been demonstrated including fork holograms [8,9] and cascaded Mach–Zehnder interferometers [10]. However, these methods are either low in efficiency or unsuitable for miniaturization and integration to realize on-chip OAM detection. In the current paper, we review the latest progress on OAM detection with the use of a plasmonic lens and grating, meta-hologram, micro-ring resonator, hybrid conformal mapper, etc. These techniques have been proven to be effective, efficient, and capable of being integrated into a compact platform.

Received April 19, 2017; accepted July 20, 2017

E-mail: qzhan1@udayton.edu

2 Plasmonics

Surface plasmon polaritons (SPPs) are the collective oscillations of free electrons, and they propagate along the metal-dielectric interface [11]. The interaction between SPPs and optical OAM states has attracted great interest recently [12,13]. Spiral phase information can be imparted onto the excited SPPs when they are excited by a vortex beam [14–16]. Light incident on a plasmonic lens made of open slots perforated in a thin metallic film either couples to SPPs propagating along the surface or directly transmits through the lens [17,18]. Evanescent SPP waves and directly transmitted propagating waves can interfere near the plasmonic lens surface and form a unique intensity distribution that is dependent on the OAM state of the

incident beam. To demonstrate this OAM detection scheme, a ring-shaped slot with a 200 nm width and a 70 nm depth is etched into the gold film by focused ion beam (FIB) lithography, forming a plasmonic lens with an inner diameter of 6 μm, as illustrated in Fig. 1 [19]. A near-field scanning optical microscope (NSOM) probe on the collection mode scans over the plasmonic lens, and near-field images of the intensity distribution of the electric field above the plasmonic lens are captured by the NSOM.

The intensity distributions are shown in Fig. 2. Because the SPPs are only excited by the locally TM polarized wave, concentric bright arcs are generated by an incident linearly polarized LG beam. For $l = 0$, corresponding to a fundamental Gaussian illumination, a solid spot appears in the center. For $|l| = 1$, a central dark spot shows up due to destructive interference. For $|l| = 2$, a bright spot reemerges. The intensity rotation direction is dependent on the sign of the topological charge: clockwise for negative charges and anticlockwise for positive charges. Light with a topological charge of $|l| > 2$ always results in a dark spot. However, the size of the central dark area can be exploited to determine the OAM mode index.

One disadvantage in plasmonic lens-based detection is the requirement of a near-field scanning mechanism to collect surface plasmons (SPs), which leads to a slow detection speed. To overcome this limit, a multi-sector meta-hologram structure with various geometrical TCs has been reported that separates the incident vortex beam into SP waves with a propagation direction depending on the OAM mode [20]. The design of the multi-sector meta-hologram is illustrated in Fig. 3. A holographic pattern with a depth of 75 nm and an area of 10 μm × 10 μm is fabricated on a gold film with a thickness of 200 nm. The holographic pattern is obtained by interfering a converging SP wave with a free-space vortex beam. The hologram is divided into four sectors with equal areas but different geometrical TCs. Assuming that a vortex beam with a TC of l_i passes through a metallic structure with a geometrical

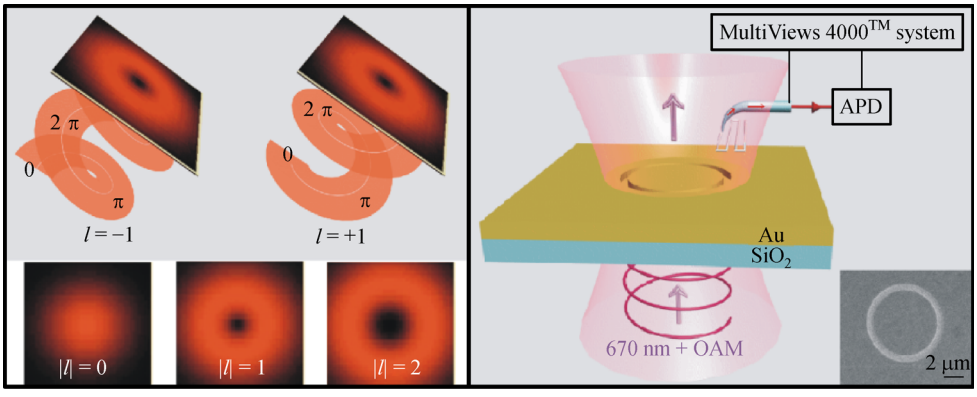

Fig. 1 (a) Schematic of light with spiral phase. The insets are the transverse intensity profiles of Laguerre-Gaussian (LG) modes with different $|l|$. (b) Schematic of experimental setup. The plasmonic lens is excited by LG modes from the SiO_2 substrate side and imaged by a NSOM probe working on collection mode. Inset 1 is the diagram of a single ring plasmonic lens and the coordinates used in analytical derivation. The illumination is along the z-direction. Inset 2 is the scanning electronic microscope micrograph of the plasmonic lens fabricated in gold film on SiO_2 substrate. Adapted from Ref. [19]

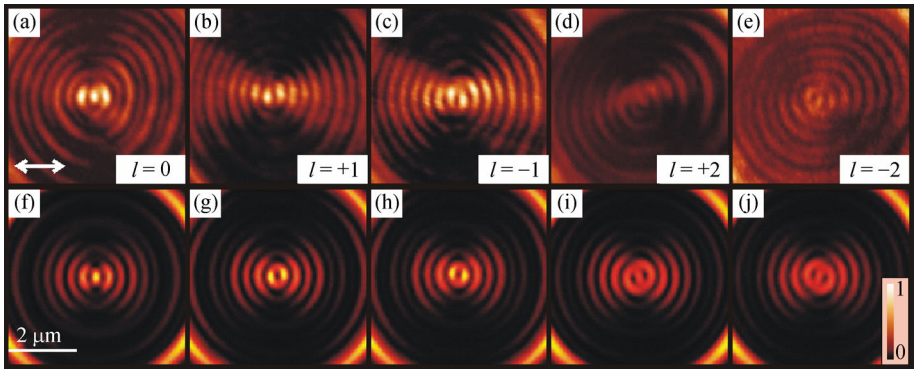

Fig. 2 Intensity distributions of the optical field near the plasmonic lens surface excited by photons with different OAMs. (a)–(e) are the NSOM images for $l = 0, +1, -1, +2$ and -2, respectively. (f)–(j) are the corresponding numerical simulation results. The excitation polarization is shown by the white arrow in (a). The scale bar in (f) and the color bar in (j) are also applicable to the other images of intensity distributions. Adapted from Ref. [19]

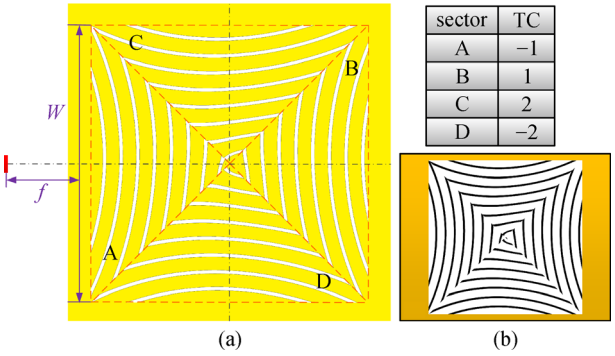

Fig. 3 (a) Schematic of the metahologram. The holographic pattern has four sectors, which are designed by considering the interference between a converging SP wave with a vortex beam carrying different OAMs. The inset corresponds to the designed TC for each sector. (b) Binary version of the interferogram. Adapted from Ref. [20]

TC of l_g, the TC of the SP wave is given by $l_s = l_i + l_g$. Consequently, different OAM modes can be differentiated when identifying the propagating direction of the SP wave because a larger l_s leads to a larger steering angle.

The number of distinguishable OAM states by the four-sector meta-hologram is estimated to be

$$N = \frac{1.22\lambda/(W/2f)}{\lambda f/(4W)} \approx 10, \tag{1}$$

where f and W are the focal length and the width of the meta-hologram, respectively. The OAM detectable range of the meta-hologram increases linearly with the number of sectors and is independent of the incident wavelength and the focal length of the hologram. Figure 4 renders the simulated near-field intensity distributions when a circular polarized vortex beam with a TC of 1 is normally incident on the meta-hologram. As expected, the illumination is

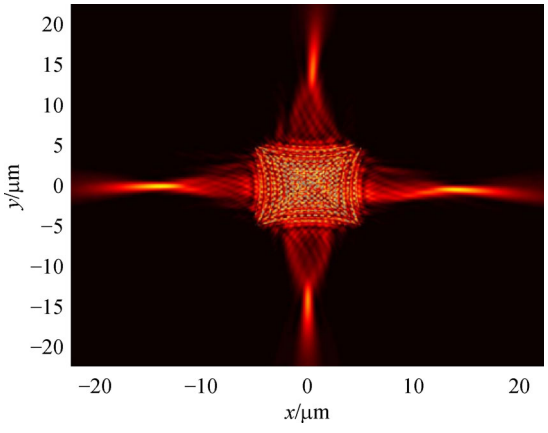

Fig. 4 Numerical simulations of the SP intensity distribution of the metahologram for circularly polarized illumination with a TC of 1. Adapted from Ref. [20]

coupled into four bunches of focused SP waves with steering angles depending on the different TCs carried by the SPs, which are (0, 2, 3, −1) for the (A, B, C, D) sectors of the meta-hologram, respectively.

A detector can be integrated into the rear side of the substrate to spatially sample the SP waves that are collected by an array of subwavelength holes with a period of 200 nm in the focal region of each channel of the meta-hologram. The data measured by the detectors are normalized to the maximum value of the signals and discretized into five levels from 0.2 to 1 with a step size of 0.2. Each level is indicated by a different color as shown in Fig. 5. Clearly, the OAM states ranging from −6 to 6 can be differentiated by the sequence of discrete signals. A higher number of OAM states can be discerned by the application of more discretization levels, as long as the signal-to-noise ratio is satisfied in practice.

Approaches based on the principle of holography have been reported to be integrated into plasmonic photodiodes and can selectively detect the orbital angular momentum of light [21]. Another intriguing alternative is to exploit plasmonic nanoantennas and convert the information on the OAM of light into spectral information using bright and dark modes [22]. All of these solutions are based on the interaction of OAM beams with plasmonics, and the sign and magnitude of topological charges are unveiled accordingly.

3 Photonic integrated circuits

With recent developments in nanotechnology, photonic integrated circuits (PICs) have been employed in a wide range of applications and have achieved multiple functionalities that were previously accomplished by bulky optical components such as ring-based Mach–Zehnder modulators [23–25]. PIC-integrated OAM detectors can be made to be very compact and efficient for OAM-based optical communication systems that have great potential in boosting the data rate.

Figure 6 shows the schematic diagram of an OAM detector that is composed of a circular resonator, angular gratings, and an access waveguide [26]. Periodic grating elements are patterned on the inner wall of the circular resonator. The width of the gratings is about 1/10 of the grating period. The periodic variation of the dielectric constant provided by the angular gratings helps couple the eigenmodes of the resonator into other modes with well-controlled OAM states [27].

When the mode matching condition is satisfied, the receiving efficiency of the device can be maximized, which is defined as the ratio of the power coupled with the access waveguide to the incident power. The coupling between the guided whispering gallery modes (WGMs) and the illumination mode can be characterized by the topological charge l of the received vortex beam:

	channel A	channel B	channel C	channel D	normalization level/a.u.
$l_i=-6$	O	R	O	B	0.54
$l_i=-5$	P	O	O	O	0.50
$l_i=-4$	B	G	O	R	1.13
$l_i=-3$	B	G	O	B	2.44
$l_i=-2$	B	O	O	B	2.93
$l_i=-1$	G	O	O	B	2.92
$l_i=0$	O	O	G	G	2.44
$l_i=1$	O	G	B	O	2.92
$l_i=2$	O	B	B	O	2.89
$l_i=3$	G	B	B	O	2.41
$l_i=4$	R	B	R	O	1.26
$l_i=5$	P	G	P	O	0.50
$l_i=6$	G	R	B	O	0.56

discretization	
B	<0.2
R	0.2–0.4
G	0.4–0.6
P	0.6–0.8
O	>0.8

Fig. 5 Lookup table for identifying incident OAM by encoding the OAM mode with discretized signal levels. Adapted from Ref. [20]

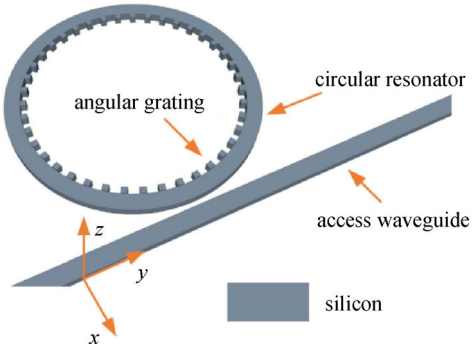

Fig. 6 Diagram of the proposed OAM receiver. The circular resonator with angular gratings patterned along the inner wall couples the normally incident azimuthally polarized vortex beam to an access waveguide. Adapted from Ref. [26]

$$l = p - g \times q, \tag{2}$$

where p and q are the number of optical periods and grating elements around the circular resonator, respectively, and g is any integer. The value of p can be calculated as

$$p = 2\pi R n_{\text{eff}}/\lambda, \tag{3}$$

where R and n_{eff} are the inner radius and the effective index of the WGM of the circular resonator, respectively. The wavelength of illumination is denoted by λ. The diffraction order g is determined by the material system [27]:

$$(n_{\text{eff}}-1)\frac{\Lambda}{\lambda} < g < (n_{\text{eff}}+1)\frac{\Lambda}{\lambda}. \tag{4}$$

When λ is around 1550 nm, R equals 3.9 μm, Λ is 598 nm, and n_{eff} is 2.6, so the value of g can only be 1. Then Eq. (2) is reduced to

$$l = p - q. \tag{5}$$

Numerical simulations are performed with a three-dimensional finite element method model (COMSOL). Figure 7 shows the receiving spectrum of the device for different OAM states from −2 to 2. The receiving efficiencies at various resonances are measured between 6% and 28%, which can be enhanced by an increase in the size of the circular resonator or an optimization of the gap distance between the resonator and access waveguide.

Considering a circularly polarized vortex beam normally illuminating the circular resonator, Eq. (5) can be rewritten according to the conservation of total angular momentum (AM) in a closed physical system:

$$j = p - q, \tag{6}$$

where $j = \sigma + l$ is the total AM and σ is the spin angular momentum. As illustrated in Fig. 8, the corresponding OAM of each resonant wavelength strongly depends on the spin of the light, making this device suitable for the identification of vortex beams with various polarization states.

GeSe is reported to support high-speed reversible transitions between phases and thus enables the reconfiguration possibility of the proposed OAM receiver [28]. As shown in Fig. 9(a), a very thin, annular photonic cap on a silicon resonator is formed by cladding a GeSe film with a thickness of 60 nm. Through doping the GeSe layer and

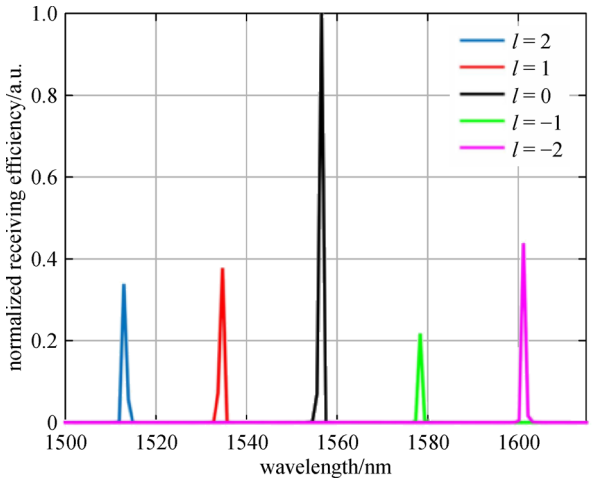

Fig. 7 Receiving spectrum of the OAM receiver. Adapted from Ref. [26]

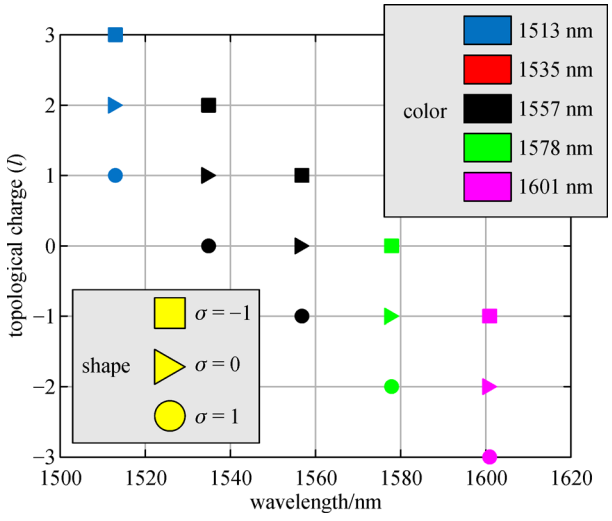

Fig. 8 Resonant wavelengths for vortex beam with different SAMs. Adapted from Ref. [26]

the lower half of the silicon resonator to provide electrical contact for both surfaces of the cladding layer, GeSe film can be pulsed with voltage for a binary phase transition. A linear and continuous phase change can be accomplished by patterning dense electrons on the GeSe film. The duty cycle of the gratings can be controlled by turning on a different number of electrodes. As an example, a 60 nm thick GeSe grating with a duty cycle of 0.5 is deposited on top of the circular resonator, and the total number of GeSe grating is chosen to be 41, as shown in Fig. 9(b).

Figure 10 shows the receiving spectrum tuned by the binary phase change of GeSe, enabling the switch of detected OAM between two different states at nearly the same wavelength. In addition, the upper cladding layer offers the function of cancelling the vertical leakage through destructively interfering the leakage propagation mode in the circular resonator, resulting in a significantly increased quality factor [29].

Integrated nanophotonic circuits have been demonstrated to be interfaced with single-mode fibers [30] to interfere with on-chip generated Gaussian beams [31] and to covert the free space vortex beam and the in-plane guiding wave to each other by introducinga holographic grating on top of a dielectric waveguide [32]. PICs have also been experimentally demonstrated for free-space spatial division-multiplexing optical transmission with multiplexed OAM states over a topological charge range of -2 to $+2$ [33]. These techniques introduce vast opportunities of integrating conventional optical systems and functionalities onto a silicon chip.

4 Spatial light modulators

Spatial light modulators (SLMs) empower researchers to have access to structured light with phase control on a pixel by pixel level. With the ingenious combination of additional optical elements, SLMs render the full control of all four degrees of freedom of a structured beam [34]. SLMs have been intensively utilized for the proof-of-

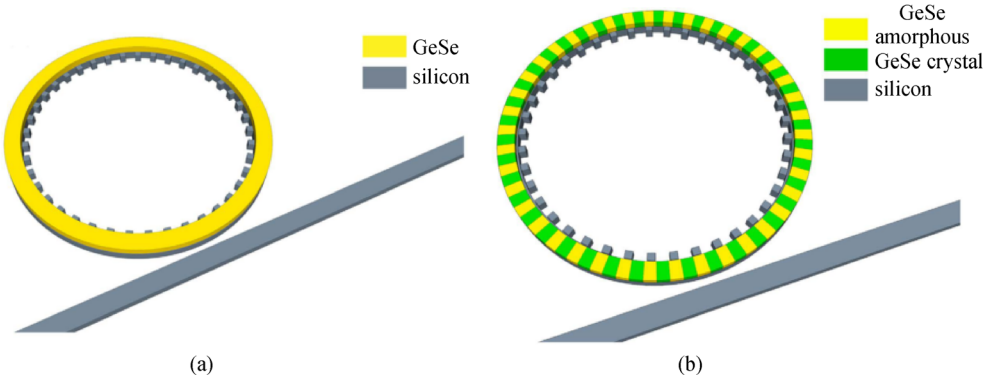

Fig. 9 Diagram of the composite OAM receiver that has a (a) GeSe annular film and (b) GeSe gratings consist of alternate states on top of the resonator as the cladding layer. The duty cycle of the gratings is 0.5. Adapted from Ref. [26]

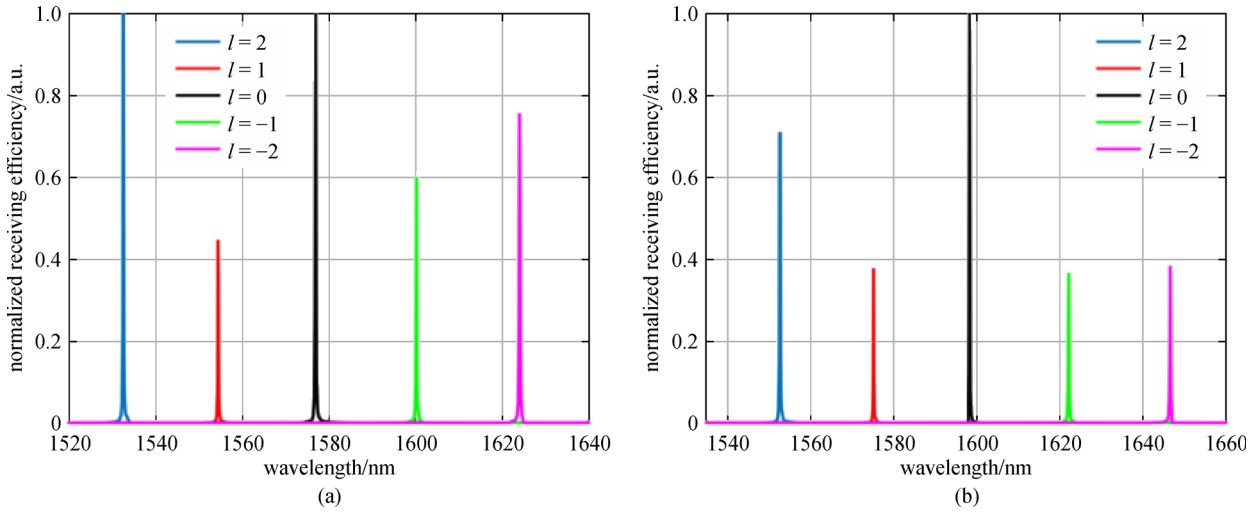

Fig. 10 Receiving spectrum of the composited device shown in Fig. 5(a) when the GeSe is in (a) amorphous state and (b) crystal state, respectively. Adapted from Ref. [26]

principle demonstration of novel OAM sorters that are promising in the integration onto a chip. The hybrid conformal mapper is one of the candidates.

Conformal mapping offers a highly efficient solution to differentiate different OAM states based on a log-polar transform [35]. The circular intensity distribution of an OAM mode is unwrapped to a straight line, and the helical phase gradient is transformed to the transverse phase gradient. However, the overlap between adjacent modes undermines the sorting resolution. To solve this problem, a fan-out element and the corresponding phase corrector can be added to the optical system to compress the width of the main lobe of each mode. Therefore, four pieces of custom diffractive and refractive optical elements with three lenses in between are implemented in the previous experimental demonstrations, as illustrated in Fig. 11(a) [36–38].

A significantly simplified high-resolution OAM sorter that comprises a quadratic fan-out mapper and a dual-

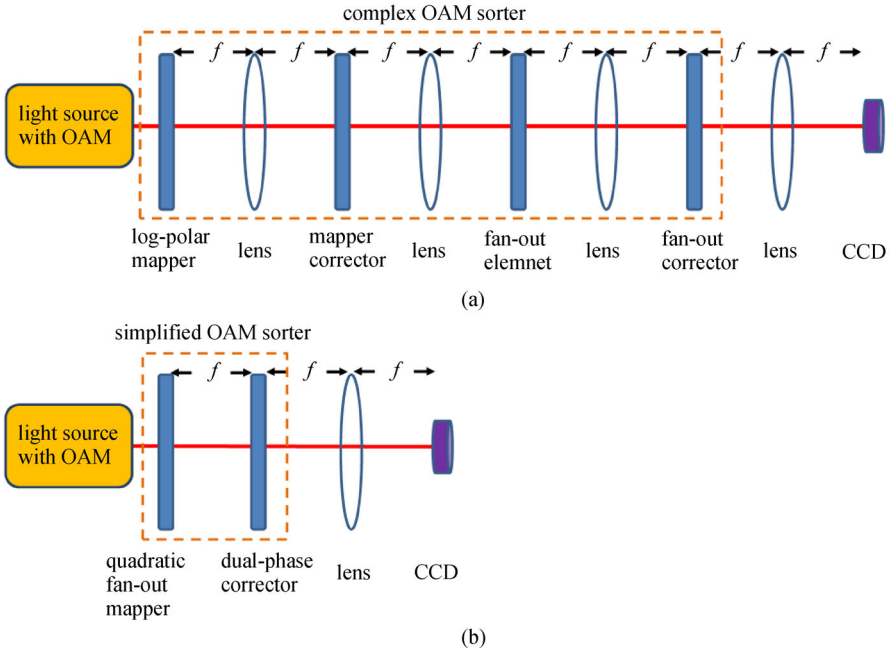

Fig. 11 Comparison of two high-resolution OAM sorters. (a) Previous demonstrations with four custom refractive/diffractive elements (log-polar mapper, mapper corrector, fan-out element, fan-out corrector) and three lenses in between. (b) The novel scheme with only two custom phase elements (quadratic fan-out mapper, dual-phase corrector) and no lens in between. Adapted from Ref. [39]

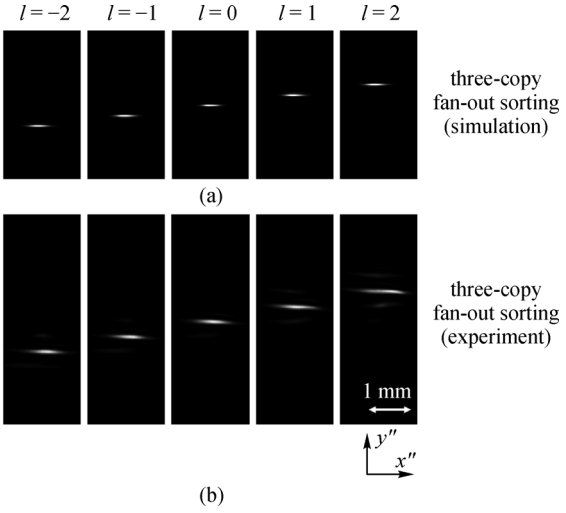

Fig. 12 Numerical simulation and experimental results for the three-copy fan-out case of OAM sorting. (a) Simulation results show that different OAM modes (l = –2, –1, 0, 1 and 2) are sorted into a set of parallel lines with various vertical positions. (b) Experimental results verify the simulation results. All experimental images use the same scale bar and coordinates. Adapted from Ref. [39]

phase corrector shown in Fig. 11(b), has recently been demonstrated [39]. The quadratic fan-out mapper simultaneously performs the log-polar transformation, fan-out beam copying, and beam focusing. The dual-phase corrector corrects both the distorted phase from the log-polar mapping and the phase jumps generated from the beam copying process.

The OAM sorter is demonstrated using a single SLM with the two-phase elements implemented on the two halves of the widescreen SLM. The simulation and experimental results for the three-copy fan-out case are presented in Figs. 12(a) and 12(b), respectively. It is clearly shown that different OAM modes (l = –2, –1, 0, 1, and 2) are sorted into a set of parallel lines with various vertical positions. The sorting resolution is proportional to the number of copies of the unwrapped beam. Because this high-resolution OAM sorter is composed of only two phase elements, it is very promising to be integrated in a compact device. In fact, a similar OAM sorter based on conformal mapping without this fan-out function has been demonstrated recently on one single piece of a refractive element [40].

With the use of SLMs, gradually changing-period gratings are demonstrated for the measurement of the OAM states from Hermite–Gaussian-like diffraction patterns [41]. Annular gratings are also reported to be capable of determining the sign and magnitude of the topological charge from the orientation and number of dark fringes [42]. The inhomogeneous and anisotropic q-plates made of liquid crystals have been exploited for the encoding and decoding in alignment-free quantum communication [43].

5 Conclusions

In conclusion, micro- and nano-structures have shown great potential in the design of compact and integrated OAM detectors. By the interaction of twisted light with plasmonic structures, PICs and novel diffractive elements unfold unprecedented properties that can be exploited to create on-chip devices capable of discerning OAM states with high fidelity. These new devices may find important applications in optical communications and quantum information processing with OAM states.

References

1. Yao A M, Padgett M J. Orbital angular momentum: origins, behavior and applications. Advances in Optics and Photonics, 2011, 3(2): 161–204
2. Allen L, Beijersbergen M W, Spreeuw R J C, Woerdman J P. Orbital angular momentum of light and the transformation of Laguerre-Gaussian laser modes. Physical Review A, 1992, 45(11): 8185–8189
3. Wang J, Yang J Y, Fazal I M, Ahmed N, Yan Y, Huang H, Ren Y, Yue Y, Dolinar S, Tur M, Willner A E. Terabit free-space data transmission employing orbital angular momentum multiplexing. Nature Photonics, 2012, 6(7): 488–496
4. Willner A E, Huang H, Yan Y, Ren Y, Ahmed N, Xie G, Bao C, Li L, Cao Y, Zhao Z, Wang J, Lavery M P J, Tur M, Ramachandran S, Molisch A F, Ashrafi N, Ashrafi S. Optical communications using orbital angular momentum beams. Advances in Optics and Photonics, 2015, 7(1): 66–106
5. Courtial J, Padgett M J. Limit to the orbital angular momentum per unit energy in a light beam that can be focused onto a small particle. . Optics Communications, 2000, 173(1–6): 269–274
6. Maurer C, Jesacher A, Bernet S, Ritsch-Marte M. What spatial light modulators can do for optical microscopy. Laser & Photonics Reviews, 2011, 5(1): 81–101
7. Dholakia K, Simpson N, Padgett M, Allen L. Second-harmonic generation and the orbital angular momentum of light. Physical Review A, 1996, 54(5): R3742–R3745
8. Mair A, Vaziri A, Weihs G, Zeilinger A. Entanglement of the orbital angular momentum states of photons. Nature, 2001, 412(6844): 313–316
9. Gibson G, Courtial J, Padgett M, Vasnetsov M, Pas'ko V, Barnett S, Franke-Arnold S. Free-space information transfer using light beams carrying orbital angular momentum. Optics Express, 2004, 12(22): 5448–5456
10. Leach J, Padgett M J, Barnett S M, Franke-Arnold S, Courtial J. Measuring the orbital angular momentum of a single photon. Physical Review Letters, 2002, 88(25): 257901
11. Shalaev V M, Kawata S. Nanophotonics with Surface Plasmons. New York: Elsevier, 2007
12. Liu A, Rui G, Ren X, Zhan Q, Guo G, Guo G. Encoding photonic angular momentum information onto surface plasmon polaritons with plasmonic lens. Optics Express, 2012, 20(22): 24151–24159
13. Gorodetski Y, Shitrit N, Bretner I, Kleiner V, Hasman E.

Observation of optical spin symmetry breaking in nanoapertures. Nano Letters, 2009, 9(8): 3016–3019
14. Kim H, Park J, Cho S W, Lee S Y, Kang M, Lee B. Synthesis and dynamic switching of surface plasmon vortices with plasmonic vortex lens. Nano Letters, 2010, 10(2): 529–536
15. Cho S W, Park J, Lee S Y, Kim H, Lee B. Coupling of spin and angular momentum of light in plasmonic vortex. Optics Express, 2012, 20(9): 10083–10094
16. Shitrit N, Bretner I, Gorodetski Y, Kleiner V, Hasman E. Optical spin Hall effects in plasmonic chains. Nano Letters, 2011, 11(5): 2038–2042
17. Yang S, Chen W, Nelson R L, Zhan Q. Miniature circular polarization analyzer with spiral plasmonic lens. Optics Letters, 2009, 34(20): 3047–3049
18. Chen W, Zhan Q. Realization of an evanescent Bessel beam via surface plasmon interference excited by a radially polarized beam. Optics Letters, 2009, 34(6): 722–724
19. Liu A P, Xiong X, Ren X F, Cai Y J, Rui G H, Zhan Q W, Guo G C, Guo G P. Detecting orbital angular momentum through division-of-amplitude interference with a circular plasmonic lens. Scientific Reports, 2013, 3(1): 2402
20. Rui G, Ma Y, Gu B, Zhan Q, Cui Y. Multi-channel orbital angular momentum detection with metahologram. Optics Letters, 2016, 41 (18): 4379–4382
21. Genevet P, Lin J, Kats M A, Capasso F. Holographic detection of the orbital angular momentum of light with plasmonic photodiodes. Nature Communications, 2012, 3: 1278
22. Kerber R M, Fitzgerald J M, Reiter D E, Oh S S, Hess O. Reading the orbital angular momentum of light using plasmonic nanoantennas. ACS Photonics, 2017, 4(4): 891–896
23. Liu A, Jones R, Liao L, Samara-Rubio D, Rubin D, Cohen O, Nicolaescu R, Paniccia M. A high-speed silicon optical modulator based on a metal-oxide-semiconductor capacitor. Nature, 2004, 427 (6975): 615–618
24. Marris-Morini D, Le Roux X, Vivien L, Cassan E, Pascal D, Halbwax M, Maine S, Laval S, Fédéli J M, Damlencourt J F. Optical modulation by carrier depletion in a silicon PIN diode. Optics Express, 2006, 14(22): 10838–10843
25. Xu Q, Schmidt B, Pradhan S, Lipson M. Micrometre-scale silicon electro-optic modulator. Nature, 2005, 435(7040): 325–327
26. Rui G, Gu B, Cui Y, Zhan Q. Detection of orbital angular momentum using a photonic integrated circuit. Scientific Reports, 2016, 6(1): 28262
27. Cai X, Wang J, Strain M J, Johnson-Morris B, Zhu J, Sorel M, O'Brien J L, Thompson M G, Yu S. Integrated compact optical vortex beam emitters. Science, 2012, 338(6105): 363–366
28. Strain M J, Cai X, Wang J, Zhu J, Phillips D B, Chen L, Lopez-Garcia M, O'brien J L, Thompson M G, Sorel M, Yu S. Fast electrical switching of orbital angular momentum modes using ultra-compact integrated vortex emitters. Nature Communications, 2014, 5: 4856
29. Yang Y, Huang Y, Guo W, Lu Q, Donegan J F. Enhancement of quality factor for TE whispering-gallery modes in microcylinder resonators. Optics Express, 2010, 18(12): 13057
30. Fontaine N K, Doerr C R, Buhl L.Efficient multiplexing and demultiplexing of freespace orbital angular momentum using photonic integrated circuits. In: Proceedings of Optical Fiber Communication Conference & Exposition. 2012, OTu1I.2
31. Sun J, Moresco M, Leake G, Coolbaugh D, Watts M R. Generating and identifying optical orbital angular momentum with silicon photonic circuits. Optics Letters, 2014, 39(20): 5977–5980
32. Liu A, Zou C, Ren X, Wang Q, Guo G. On-chip generation and control of the vortex beam. Applied Physics Letters, 2016, 108(18): 181103
33. Su T, Scott R P, Djordjevic S S, Fontaine N K, Geisler D J, Cai X, Yoo S J B. Demonstration of free space coherent optical communication using integrated silicon photonic orbital angular momentum devices. Optics Express, 2012, 20(9): 9396–9402
34. Han W, Yang Y, Cheng W, Zhan Q. Vectorial optical field generator for the creation of arbitrarily complex fields. Optics Express, 2013, 21(18): 20692–20706
35. Berkhout G C, Lavery M P, Courtial J, Beijersbergen M W, Padgett M J. Efficient sorting of orbital angular momentum states of light. Physical Review Letters, 2010, 105(15): 153601
36. Malik M, Mirhosseini M, Lavery M P, Leach J, Padgett M J, Boyd R W. Direct measurement of a 27-dimensional orbital-angular-momentum state vector. Nature Communications, 2014, 5: 3115
37. O'Sullivan M N, Mirhosseini M, Malik M, Boyd R W. Near-perfect sorting of orbital angular momentum and angular position states of light. Optics Express, 2012, 20(22): 24444–24449
38. Mirhosseini M, Malik M, Shi Z, Boyd R W. Efficient separation of the orbital angular momentum eigenstates of light. Nature Communications, 2013, 4: 2781
39. Wan C, Chen J, Zhan Q. Compact and high-resolution optical orbital angular momentum sorter. APL Photonics, 2017, 2(3): 031302
40. Ruffato G, Massari M, Romanato F. Compact sorting of optical vortices by means of diffractive transformation optics. Optics Letters, 2017, 42(3): 551–554
41. Dai K, Gao C, Zhong L, Na Q, Wang Q. Measuring OAM states of light beams with gradually-changing-period gratings. Optics Letters, 2015, 40(4): 562–565
42. Zheng S, Wang J. Measuring orbital angular momentum (OAM) states of vortex beams with annular gratings. Scientific Reports, 2017, 7: 40781
43. D'Ambrosio V, Nagali E, Walborn S P, Aolita L, Slussarenko S, Marrucci L, Sciarrino F. Complete experimental toolbox for alignment-free quantum communication. Nature Communications, 2012, 3: 961

Chenhao Wan obtained the Ph.D. degree in Electrical Engineering from the University of Minnesota. Currently he is a faculty member in the School of Optical and Electronic Information at Huazhong University of Science and Technology. His research interests range from coherent beam combining and polarization gratings to tailoring structured light.

Guanghao Rui received the Ph.D. degree in Optics from the Department of Optics and Optical Engineering at University of Science and Technology of China in 2013. He is currently an Associate Professor at the School of Electronic Science & Engineering, Southeast University, Jiangsu, China. He was a Visiting Scholar and Research Scientist in the Department of Electro-Optics and Photonics at University of Dayton from 2010 to 2012, and from 2013 to 2014, respectively. His research interests include nanophotonics, plasmonics, metasurfaces, optical tweezers and complex optical field. Dr. Rui is a member of the Optical Society of America, director and vice secretary general of the Jiangsu Optical Society.

Jian Chen received the B.S. degree from Southwest University of Science and Technology in 2011. He is now a Ph.D. student for signal and information processing at University of Electronic Science and Technology of China, and studying in the University of Dayton through joint training program sponsored by the China Scholarship Council. His research interests are mainly in achieving spatial engineering of light wave properties (including polarization, intensity and phase) based on liquid crystal spatial light modulators.

Prof. **Qiwen Zhan** received his B.S. degree in Physics (Optoelectronics) from the University of Science and Technology of China in 1996 and Ph.D. degree in Electrical Engineering from the University of Minnesota in 2002. The current research in his group mainly focuses on developing new polarization engineering techniques and exploring their applications in nanophotonics, metrology, and biophotonics. Dr. Zhan is an Associate Editor for *Optica* (OSA), Member of the Editorial Board for *Sceintific Reports* (Nature Publishing Group) and the *Journal of Nondestructive Evaluation* (Nature Springer). He is elected Fellow of the OSA, Fellow of the SPIE, and Senior Member of the IEEE.